

©2003 IEEE. Personal use of this material is permitted. However, permission to reprint/republish this material for advertising or promotional purposes or for creating new collective works for resale or redistribution to servers or lists, or to reuse any copyrighted component of this work in other works must be obtained from the IEEE.

Copyright and all rights therein are retained by authors or by other copyright holders. All persons copying this information are expected to adhere to the terms and constraints invoked by each author's copyright. In most cases, these works may not be reposted without the explicit permission of the copyright holder.

This copyright notice is taken from the IEEE PSPB Operations Manual, section 8.1.10 entitled "Electronic Information Dissemination". At the time of this notice, this section is posted at

[http://www.ieee.org/portal/index.jsp?pageID=corp\\_level1&path=about/documentation/copyright&file=policies.xml&xsl=generic.xsl](http://www.ieee.org/portal/index.jsp?pageID=corp_level1&path=about/documentation/copyright&file=policies.xml&xsl=generic.xsl)

# Tunable Coupled Inductor $Q$ -Enhancement for Parallel Resonant $LC$ Tanks

Bogdan Georgescu, *Student Member, IEEE*, Holly Pekau, *Student Member, IEEE*, James Haslett, *Fellow, IEEE*, and John McRory, *Member, IEEE*

**Abstract**—A tunable transformer-based  $Q$ -enhancement method for monolithic inductors used in parallel resonant  $LC$  tanks is presented. The  $Q$  of the inductor that forms the transformer primary is enhanced by cancelling the voltage drop across the series loss resistance of the primary with a voltage of opposite polarity that is induced by a current in the secondary. The circuit allows dc voltage control of  $Q$ -enhancement. Techniques to address stability issues associated with the positive feedback are described. The circuit was fabricated in 0.18- $\mu\text{m}$  CMOS and the performance was verified experimentally.

**Index Terms**—CMOS, distortion,  $LC$  filters, monolithic, noise,  $Q$ -enhancement, transformer.

## I. INTRODUCTION

THE GROWTH of modern communications systems operating at radio frequencies has led to the development of highly integrated transceivers. One of the factors limiting the integration of RF transceivers is the low quality of the passive components in commercially available IC processes. An important example of this is the limited integration of RF filters because the quality factor of monolithic spiral inductors is very low. These inductors are inherently lossy due to ohmic losses in the metal traces and due to substrate resistance and eddy currents. This problem has been addressed by using various passive methods such as patterned ground shields and geometry improvements [1], [2], but the  $Q$  factor of integrated inductors is still generally limited to a value less than 20 [3] in standard RF-CMOS processes. To realize acceptable monolithic filters requires inductors with significantly higher- $Q$  factors [4]. Many active circuits that realize inductive impedance characteristics have been proposed as a solution to the problem. The inductance realized by these circuits is proportional to a capacitance and inversely proportional to the square of a transconductance, necessitating relatively high-bias currents to achieve small inductance values at RF. This results in significant power consumption and noise. A third solution is to enhance the  $Q$  of lossy integrated inductors with an active circuit. Many active  $Q$ -enhancement techniques that use positive feedback to generate a negative re-

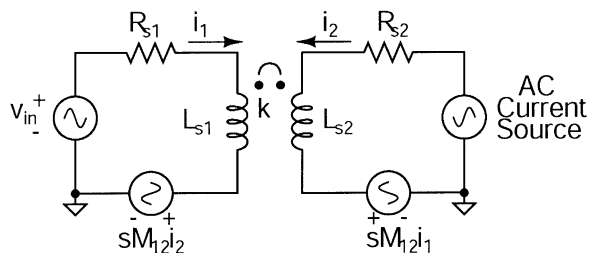


Fig. 1. Transformer based  $Q$ -enhancement principle.

sistance that cancels the inductor loss resistance have been proposed [5], [6].

Transformer based  $Q$ -enhancement techniques have demonstrated good performance at radio frequencies [7]–[9], [4]. The principle of these techniques is illustrated in Fig. 1. By inspection

$$v_{in} = i_1 R_{s1} + i_1 s L_{s1} + i_2 s M_{12} \quad (1)$$

where  $M_{12} = k\sqrt{L_{s1}L_{s2}}$  is the mutual inductance between the windings and  $k$  is the coupling coefficient. In order for the input impedance of the circuit to be purely inductive,  $Re(i_1 R_{s1} + s M_{12} i_2) = 0$ . Previous authors have shown that an appropriate choice of  $i_2$  will cancel the loss and enhance the inductance. At RF frequencies, the primary goal is to cancel the loss. Setting  $i_1 R_{s1} = -i_2 s M_{12}$  results in  $i_1 = v_{in}/(s L_{s1})$ , which corresponds to a lossless inductor of value  $L_{s1}$ . The required secondary current is

$$i_2 = \frac{-i_1 R_{s1}}{s M_{12}} = \frac{-v_{in} R_{s1}}{s^2 M_{12} L_{s1}}. \quad (2)$$

Rewriting with  $s = j\omega$  results in

$$i_2 = \frac{v_{in} R_{s1}}{\omega^2 k L_{s1} \sqrt{L_{s1} L_{s2}}}. \quad (3)$$

For a unity turns ratio transformer,  $L_{s1} = L_{s2} = L_s$  and  $R_{s1} = R_{s2} = R_s$ . Then (3) reduces to

$$i_2 = \frac{v_{in} R_s}{k \omega^2 L_s^2} = \frac{v_{in}}{k Q^2 R_s} \quad (4)$$

where  $Q = \omega L_s / R_s$  is the uncompensated quality factor of the primary and secondary inductors. From (3) it can be seen that  $i_2$  is a current that is in phase with the primary voltage and can be readily implemented in circuit form at radio frequencies. The idea was described by Pehlke *et al.* using external instrumentation in 1997 [7]. A novel implementation using a pMOS current mirror to drive the secondary was proposed by Wu and Chang

Manuscript received March 31, 2003; revised July 30, 2003. This work was supported in part by the Natural Sciences and Engineering Research Council of Canada, in part by the Alberta Informatics Circle of Research Excellence, in part by TRILabs, the University of Calgary, and in part by the Canadian Microelectronics Corporation. This paper was recommended by Associate Editor J. Silva-Martinez.

B. Georgescu, H. Pekau, and J. Haslett are with the University of Calgary, Department of Electrical and Computer Engineering, Calgary, AB T2N 1N4, Canada (e-mail: haslett@enel.ucalgary.ca).

J. McRory is with TRILabs, Calgary, AB T2L 2K7, Canada.

Digital Object Identifier 10.1109/TCSII.2003.818366

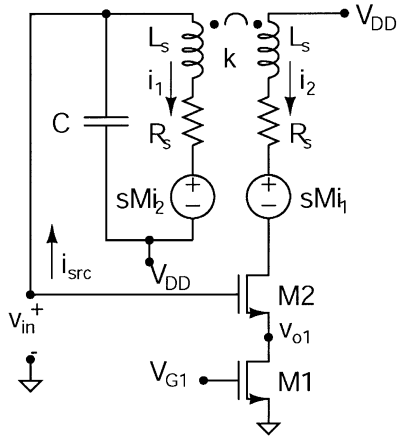


Fig. 2. Circuit implementation of transformer based  $Q$ -enhancement for a monolithic inductor in a parallel resonant  $LC$  tank.

[8], which requires an additional phase-shifting capacitor and has some added noise from the mirror transistors. An implementation in a bootstrapped LNA application was described by Albertoni *et al.* [9]. The circuit achieved a maximum  $Q$  of 30, and was fabricated in a bipolar process. Soorapanth and Wong [4] suggested an implementation that used a capacitor in series with the primary such that the required current in the secondary was proportional to  $1/j\omega$ . This implementation makes the compensating induced voltage in the primary independent of frequency, a result that is useful in filter applications where a flat passband is desirable. The series-resonant  $LC$  circuit in the implementation proposed in [4] requires a particular filter topology. This paper describes a tunable implementation of the  $Q$ -enhancement method with low transistor count, applied to parallel resonant tank circuits. Noise, distortion, and stability are addressed. The tunable enhanced resonant tank allows the exploration of new active filter topologies.

## II. CIRCUIT IMPLEMENTATION

The circuit implemented in this work is shown in Fig. 2. The compensating current,  $i_2$ , in the secondary is generated by the M1-M2 FET circuit, which is driven by the input voltage,  $v_{in}$ . M1 operates in triode, and the gate voltage of M1 is used to control the amount of  $Q$ -enhancement.

A detailed analysis of the electrical behavior of the circuit including all transconductances, output conductances and parasitic capacitances is complex. In order to obtain a physical appreciation of circuit behavior, we assume that  $g_{ds2} = 0$  and ignore the effects of  $g_{mb2}$  and  $C_{db1,2}$ . We have found that this approach adequately models the first order behavior of the circuit.

With these assumptions, the compensating current is given by

$$i_2 = v_{o1}g_{ds1} = \frac{g_{m2}v_{in}}{1 + g_{m2}/g_{ds1}}. \quad (5)$$

Summing currents at the  $v_{in}$  node gives

$$i_{src} = v_{in}sC + \frac{(v_{in} - sMi_2)}{R_s + sL_s}. \quad (6)$$

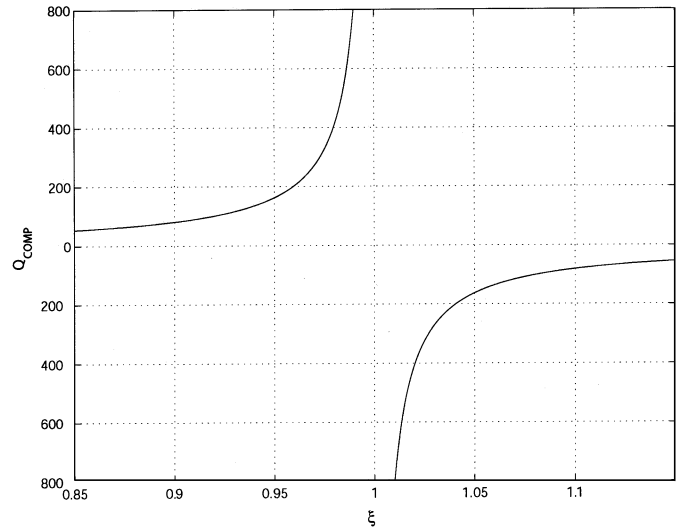


Fig. 3. Enhanced  $Q$  versus compensating current error factor,  $\xi$ , with  $Q = 8$ .

From (6) the input impedance of the resonant tank is

$$\frac{v_{in}}{i_{src}} = Z_{in} = \frac{R_s + sL_s}{s^2L_sC + s(R_sC - G_mL_s) + 1} \quad (7)$$

where

$$G_m = \frac{ki_2}{v_{in}} = \frac{kg_{ds1}}{1 + g_{ds1}/g_{m2}}. \quad (8)$$

From (7) it can be shown that the compensated  $Q$  factor is approximately given by

$$Q_{COMP} = \frac{1}{\omega_{res}R_sC \left(1 - \frac{G_mL_s}{R_sC}\right)} \quad (9)$$

where  $\omega_{res} = 1/\sqrt{L_sC}$ . For infinite  $Q$  at  $\omega_{res}$

$$G_m = \frac{R_s}{(\omega_{res}L_s)^2} = \frac{R_sC}{L_s}. \quad (10)$$

Compensation of the voltage drop across the loss resistance of the primary is exactly correct only if (3) is satisfied. The general behavior of the compensated  $Q$  of the circuit can be analyzed by using an error factor,  $\xi$ , in the secondary compensating current

$$i_2 = +\xi \frac{v_{in}R_s}{k\omega^2L^2}. \quad (11)$$

When  $\xi = 1$ , the  $Q$  of the compensated inductor is infinite. When  $\xi \neq 1$ , it can be shown that

$$Q_{COMP}(\xi) = \frac{Q}{(1 - \xi)} \left(1 + \frac{\xi}{Q^2}\right). \quad (12)$$

Fig. 3 shows a plot of  $Q_{COMP}$  versus  $\xi$  for a transformer with uncompensated primary and secondary  $Q$  factors of 8. It can be seen that the enhanced  $Q$  is still fairly high ( $Q_{COMP} \sim 80$ ) for a 10% error in the compensating current.

From (12), it can be seen that  $Q$  can be made negative if  $\xi > 1$ , allowing other losses to be compensated if they appear in parallel with the transformer primary coil.

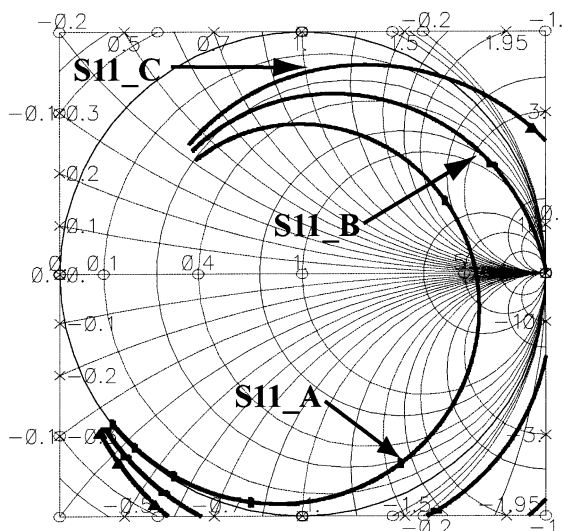


Fig. 4.  $S_{11}$  of  $Q$ -enhanced parallel resonant tank:  $S_{11\_A}$ : the enhanced  $Q$  is low and the circuit is stable,  $S_{11\_B}$ : the enhanced  $Q$  is very high and  $|S_{11}| < 1$  at  $\omega_{res}$  but the circuit may have a stability issue due to nonlinear effects,  $S_{11\_C}$ :  $|S_{11}| > 1$  at  $\omega_{res}$  and the circuit will oscillate.

#### A. Stability Analysis

The use of positive feedback to compensate the loss resistance of an inductor can result in potential instability depending on the circuit terminating impedances. In addition, process and temperature variations will result in shifts in the enhanced  $Q$  of the circuit requiring additional self-tuning circuitry to compensate for these variations. If the circuit is employed in a filter, the filter might be stable even though the unloaded tank has an input reflection coefficient greater 1. In order to make sure the circuit is stable for all terminating impedances with input reflection coefficients less than 1, it is enough to ensure that the magnitude of the input reflection coefficient associated with the unloaded tank is less than 1 for all frequencies.

From (7) using a linear analysis the circuit will be stable provided that

$$G_m \leq \frac{R_s C}{L_s}. \quad (13)$$

If a more complete high-frequency model of the circuit is used, then the Nyquist criterion or the Smith Chart can be used to analyze the stability of the circuit. In terms of the Smith Chart, oscillation of the unloaded tank will occur if the absolute value of the input reflection coefficient,  $|S_{11}| > 1$  at  $\omega_{res}$  as shown in Fig. 4.

The condition described in (13) assumes linear behavior of the feedback circuit. Several nonlinear effects may occur in practice. If the enhanced  $Q$  is sufficiently high,  $|S_{11}|$  can be less than 1 at  $\omega_{res}$  but greater than 1 for some frequency greater than  $\omega_{res}$  because the compensating voltage in the primary is proportional to  $\omega^2$ . In this case, the circuit may oscillate due to nonlinear effects even though the linear stability condition is satisfied.

Nonlinear effects occur because of the variation of  $g_{ds1}$  and  $g_{m2}$  at large signal swings. These variations cause  $G_m$  to vary with the voltage across the tank, and can cause oscillation if a

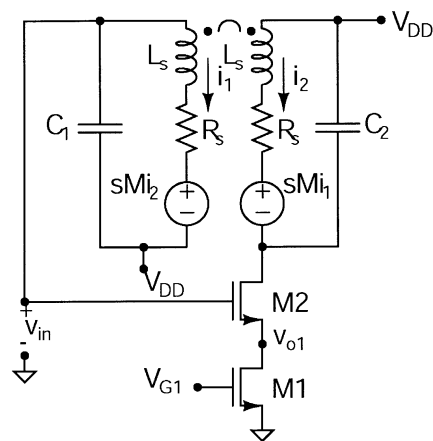


Fig. 5. Stabilization method using a capacitor to resonate the secondary.

large signal is applied. We have found that this nonlinear effect may be mitigated by modestly increasing the loss resistance of the secondary coil, without sacrificing  $Q$  tunability and enhancement.

Oscillation may also occur if the tank is reactively loaded such that the resonant frequency increases to a value where  $|S_{11}| > 1$ .

The stability problem due to the frequency dependence and the nonlinear nature of the positive feedback can be addressed by using various techniques. One such technique is to resonate the secondary inductance with a parallel capacitor, as shown in Fig. 5. This reduces the amount of small signal compensating current flowing through the secondary inductor at high frequencies so that the amount of loss compensation at high frequencies is reduced, stabilizing the circuit. While this allows the circuit to be stabilized, it has a significant effect on the resonant frequency of the primary tank. If the enhanced  $Q$  is high then a good approximation of the resulting resonant frequency of the primary is

$$f_{res} \approx \frac{1}{2\pi \sqrt{L_s(C_1 + C_2) + C_1 C_2 R_s^2}}. \quad (14)$$

It should be noted that the transformer parasitic capacitances and the drain-bulk capacitance of M2 are considered, when choosing  $C_1$  and  $C_2$ . In practice the transistor drain-bulk capacitances have a negligible effect on circuit performance, but the parasitic transformer capacitances can be significant.

An alternative technique is to introduce a resonant tank in the source of the triode FET, M1, as shown in Fig. 6. This stabilizing tank circuit is designed to resonate at a frequency higher than the primary resonance, so that the follower gain, and the corresponding compensating current are reduced at frequencies above the primary resonance. The stabilized  $S_{11}$  plots using each of the two proposed stabilization methods are shown in Fig. 7.

#### B. Noise Analysis

To facilitate a theoretical noise analysis of the circuit, an appropriate noise model for the FETs is required. There is signif-

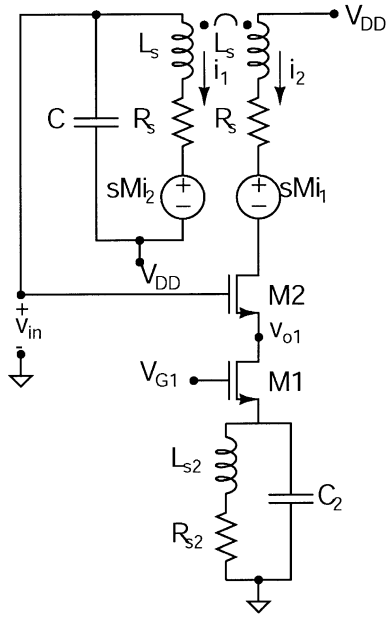


Fig. 6. Stabilization method using a resonant tank in the source of M1.

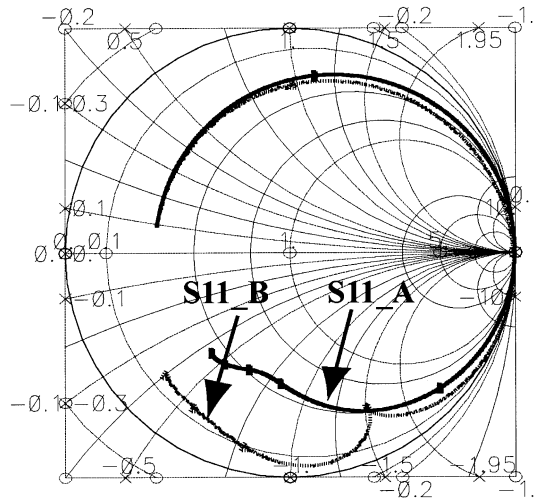


Fig. 7. Stabilized S11: S11\_A with resonating capacitor in parallel with secondary coil, S11\_B with parallel resonant LC tank in source of M1.

icant literature on the topic. An accepted expression for FET thermal drain noise current is [10]

$$\frac{\bar{i}_d}{\sqrt{\Delta f}} = \sqrt{\gamma 4kTg_{d0}} \quad (15)$$

where  $g_{d0}$  is the drain-source conductance at zero  $V_{ds}$  and  $\gamma$  is chosen empirically to match the observed noise behavior of a given fabrication process. Quite often circuit simulators replace  $g_{d0}$  with  $g_m$ , which is strictly valid only for long channel devices. Theoretically,  $\gamma = 2/3$  for long channel devices. Recent work by Scholten *et al.* [11] suggests that  $\gamma$  may be close to  $2/3$  even for short channel devices. Nicollini [12] has shown that the following expression agrees closely with measurements on long channel devices, and is in common use for Level 1 FET models in circuit simulators

$$\frac{\bar{i}_{d1}}{\sqrt{\Delta f}} = \sqrt{\gamma 4kT(g_m + g_{mb} + g_{ds})}. \quad (16)$$

In order to facilitate comparison of theory with simulation and to gain a physical understanding of the dominant noise sources and their functional dependence on circuit parameters, the Nicollini model is used in the following sections.

The noise voltage that appears at the input terminals of the tank across an arbitrary source resistance  $R_{src}$  is of interest. Using superposition we analyze the contribution to this equivalent input referred noise voltage from each noise source in the circuit. The three main noise sources are the thermal noise of  $R_s$  in the primary, and the thermal drain current noises of M1 and M2, taking the internal feedback into account. Once again, we neglect  $g_{ds2}$  and  $g_{mb2}$  for simplicity. For the case where there is no additional stabilization circuitry, we can neglect the thermal noise contribution from  $R_s$  in the secondary because  $g_{ds2}$  is zero.

The contribution of the thermal noise of  $R_s$  may be analyzed using the circuit of Fig. 8(a). The contributions of the thermal drain noise currents of M1 and M2 may be analyzed by examining Fig. 8(b) and (c), respectively.

The noise contributions of  $R_s$ , M1, and M2 are shown in Table I, where

$$D = s^2 + s \left( \frac{1}{CR_{src}} + \frac{R_s}{L_s} - \frac{G_m}{C} \right) + \frac{R_s + R_{src}}{L_s CR_{src}}. \quad (17)$$

It should be noted that  $D$  tends toward a low value at resonance for high  $Q$ , so that the noise in the circuit at the resonant frequency is significantly increased as  $Q$  is raised.

The calculated noise contributions are plotted in Fig. 9 for the case where  $L_s = 6$  nH,  $C = 2$  pF,  $R_s = 10$   $\Omega$ ,  $g_{m2} = 0.024$  S,  $g_{m1} = 0.031$  S,  $g_{ds1} = 0.0037$  S,  $Q = 150$ ,  $V_{DD} = 3$  V,  $R_{src} = \infty$ . These results agree with simulated results using a simple lumped element transformer model and Level 1 FET models with  $\gamma = 2/3$ . It can be seen that the main contributor to the total input referred noise is the triode FET, M1.

The maximum noise is of interest when considering the use of the actively compensated inductance in a circuit application. The worst case noise voltage across the tank will occur when  $R_{src} = \infty$ . Using the equations in Table I, the peak noise due to M1, M2, and  $R_s$  can be written in terms of the compensated  $Q$  factor,  $Q_{COMP}$  as

$$\frac{\bar{v}_{in}}{\sqrt{\Delta f}} = K \sqrt{\frac{\bar{i}_{d1}^2}{\Delta f} \cdot \frac{1}{g_{ds1}^2} + \frac{\bar{i}_{d2}^2}{\Delta f} \cdot \frac{1}{g_{m2}^2} + \frac{\bar{e}_n^2}{\Delta f} \cdot \frac{C}{L_s G_m^2}} \quad (18)$$

where  $K$  is a dimensionless constant given by

$$K = G_m Q_{COMP} \sqrt{\frac{L_s}{C}}. \quad (19)$$

The terms inside the square root of (18) represent the peak noise contributions of M1, M2, and  $R_s$ , respectively, as shown in Fig. 9.

It was previously shown that the  $Q$ -enhancement circuit has a stability issue due to the frequency dependence of the positive feedback and two possible methods of stabilizing it were proposed 1) resonating the transformer secondary with a capacitor and 2) degenerating the source of M1 with a resonant tank. Resonating the secondary with a capacitor results in a total input referred noise similar to the case with no stabilization. When the

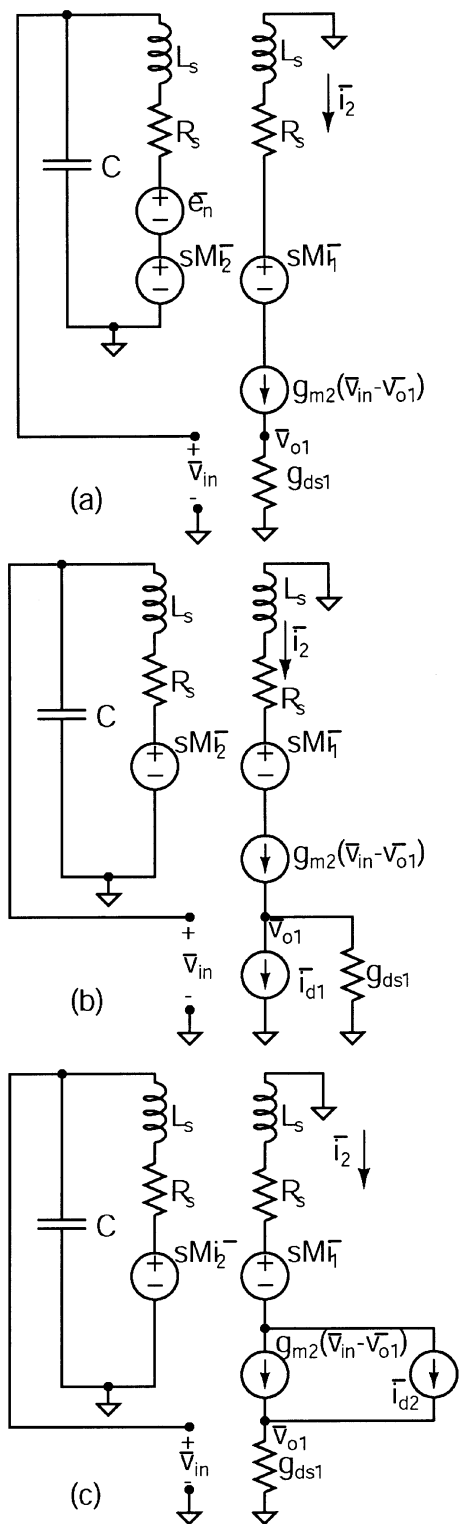


Fig. 8. Equivalent circuit for calculating input referred noise contribution of (a)  $R_s$ , (b) M1, and (c) M2 with  $R_{src} = \infty$ .

secondary capacitance is present, the secondary loss resistance contributes to the input referred noise. However, to maintain the same resonant frequency, the primary capacitance is reduced. The net result is that the overall input referred noise does not change appreciably from the case when the secondary capacitor is not present.

TABLE I  
NOISE CONTRIBUTIONS OF  $R_s$ , M1, AND M2, TO THE INPUT REFERRED NOISE,  $v_{in}$

	Thermal noise generated	Contribution to $\bar{v}_{in}$
$R_s$	$\frac{\bar{\epsilon}_n}{\sqrt{\Delta f}} = \sqrt{4kTR_s}$	$\frac{\frac{\bar{\epsilon}_n}{\sqrt{\Delta f}}/L_s C}{D}$
M1	$\frac{\bar{i}_{d1}}{\sqrt{\Delta f}} = \sqrt{\gamma 4kT(g_{m1} + g_{ds1})}$	$\frac{\frac{\bar{i}_{d1}}{\sqrt{\Delta f}} \frac{sG_m}{Cg_{ds1}}}{D}$
M2	$\frac{\bar{i}_{d2}}{\sqrt{\Delta f}} = \sqrt{\gamma 4kTg_{m2}}$	$\frac{\frac{\bar{i}_{d2}}{\sqrt{\Delta f}} \frac{sG_m}{Cg_{m2}}}{D}$

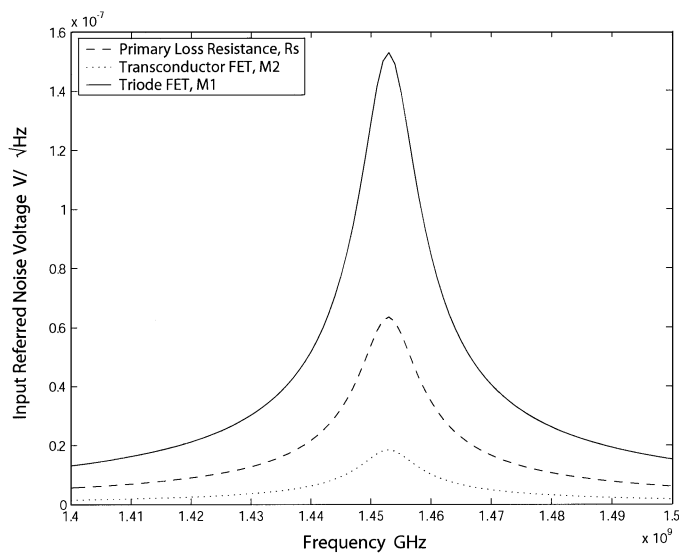


Fig. 9. Simulated input referred noise contributions for  $R_s$ , M1, and M2.

The simulated noise contributions of  $R_{s1}$ ,  $R_{s2}$ , M1, and M2 to the input referred noise voltage for the circuit with a resonated secondary with  $L = 6$  nH,  $C_1 = 650$  fF,  $C_2 = 1.3$  pF,  $R_{s1} = R_{s2} = 10$   $\Omega$ ,  $g_{m2} = 0.0239$  S,  $g_{m1} = 0.0320$  S,  $g_{ds1} = 0.0018$  S,  $Q = 150$ ,  $V_{DD} = 3$  V,  $R_{src} = \infty$  are shown in Fig. 10.

The second proposed stabilization technique based on placing a resonant tank in the source of M1 does not change the input referred noise significantly near resonance because the impedance of the stabilizing tank is low, near the resonant frequency of the primary tank.

Although the above noise analysis uses simplified models to gain physical insight into the contributions of the various noise sources, a more complete noise modeling approach including all parasitics yields similar results. The peak noise in the detailed simulation is within 10% of that predicted by the simple analysis for the examples shown. It should be noted that in practice  $\gamma$  in (15) can be significantly higher than the Level 1 simulator model resulting in an increased noise level above that predicted by the Level 1 models.

### C. Linearity Analysis

The main sources of nonlinearity in the circuit are the FETs M1 and M2. In addition to nonlinearities arising due to deviations from the ideal small signal behavior, further nonlinearities

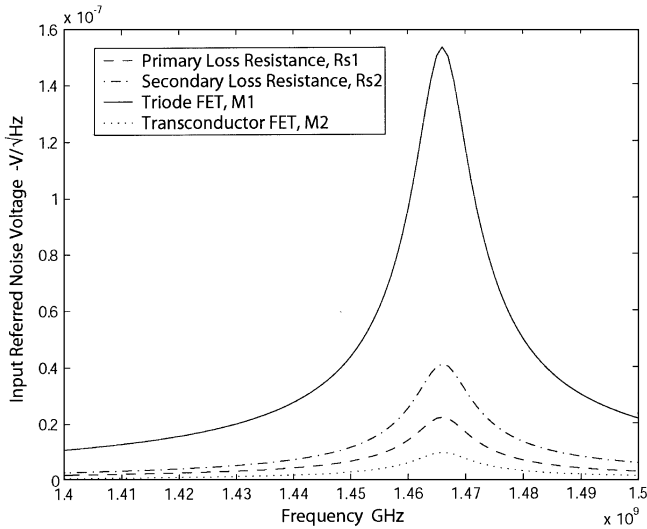


Fig. 10. Simulated input referred noise contributions for  $R_{s1}$ ,  $R_{s2}$ , M1, and M2 with resonated transformer secondary.

will occur when M1 is pulled into saturation and M2 into triode at large signal swings. This is due to the relatively high compensating current swings required in the secondary winding to attain high  $Q$  values. For a realistic case where  $L = 4$  nH,  $k = 0.8$ , and  $R_s = 11 \Omega$  with the circuit operating at 1.6 GHz, the amplitude of the compensating current for a 100-mV input is 0.85 mA, according to (3). The linearity may be improved if the quality of the transformer windings is good along with a good coupling factor.

The  $Q$ -enhanced inductor is a 1-port device, making it difficult to apply conventional measures of linearity such as IP3 and P1 dB, which are geared toward a 2-port system. The  $Q$ -enhancement circuit may be considered as a voltage input—current output device. In simulation, a measure of the linearity of the  $Q$ -enhanced inductor can be obtained by applying a voltage drive from a zero impedance source and observing the harmonic content of the input current. In practice, an ideal voltage source cannot be used to drive the tank and the harmonic content of the input current is difficult to measure directly. An alternative experimental method to measure the linearity performance of the circuit is described in Section III.

### III. EXPERIMENTAL RESULTS

The circuit of Fig. 2 was implemented in a 0.18- $\mu\text{m}$  CMOS logic process with a low-resistivity epitaxial substrate. A logic process was selected for the implementation because the passive inductors fabricated using this process would have a very low  $Q$  in the range of 1 to 2, allowing the capabilities of the  $Q$ -enhancement method to be fully demonstrated. As this was a proof of concept of the tunable parallel resonant coupled inductor  $Q$ -enhancement method, and since there was no load defined for the circuit, no stabilization method was used in the actual circuit implementation. A die micrograph of the circuit is shown in Fig. 11. The circuit consumes 5 mA from a  $V_{DD} = 1$  V supply for a 5 mW total with  $V_{G1} = 1.65$  V. The power consumption would be greatly reduced if the circuit was implemented on a low-loss nonepitaxial substrate.

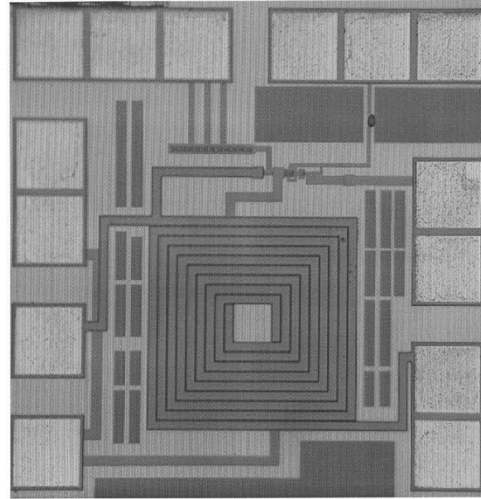


Fig. 11. Die micrograph—size  $650 \mu\text{m} \times 650 \mu\text{m}$ .

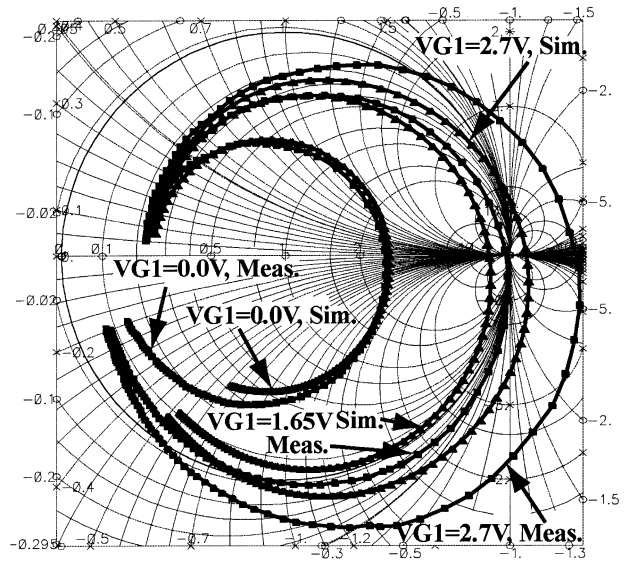


Fig. 12. Simulated versus measured S11 for various gate control voltages.

#### A. S11 Measurement

The input reflection coefficient of the  $Q$ -enhanced parallel resonant tank was measured using an HP8510 Network Analyzer and a Cascade Microtech Wafer Prober. Fig. 12 shows the measured and simulated S11 traces for different values of the enhanced  $Q$ , corresponding to different gate voltages applied to the triode FET, M1. Fig. 13 shows the measured absolute values of the tank input impedance for different values of the enhanced  $Q$ , corresponding to different gate voltages applied to the triode FET, M1. The simulated curves in Fig. 12 were generated using a full layout simulation of the passive components, including the pads, the transformer, and the interconnects in HP ADS Momentum, a 2.5D electromagnetic modeler. The discrepancy in the measured and the simulated results is primarily due to the lack of an accurate substrate model for the CMOS logic process that was used to fabricate the circuit. However, the tunable  $Q$ -enhancement is clearly demonstrated, with  $Q$  approaching infinity for  $V_{G1} > 1.7$  V.

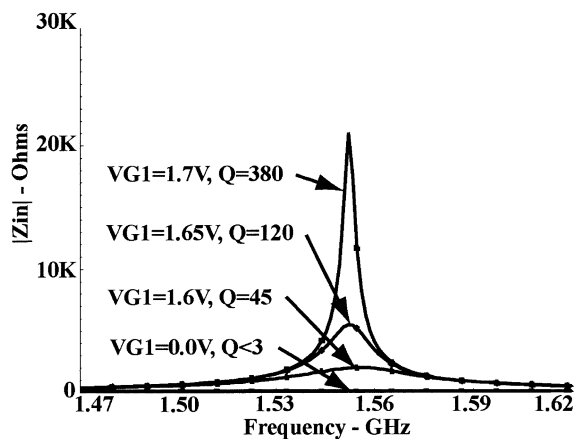


Fig. 13. Measured  $|Z_{in}|$  for various gate control voltages.

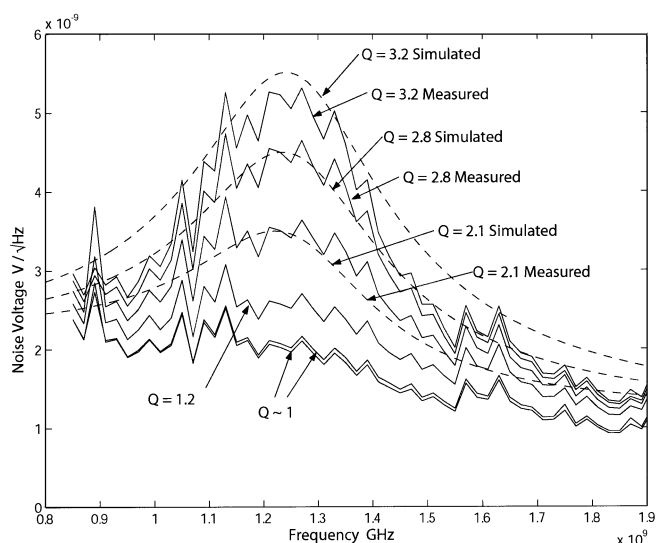


Fig. 14. Measured noise versus frequency at the output of the npn buffer for various loaded  $Q$ s (simulated results shown for  $Q = 3.2, 2.8, 2.1$ ).

**B. Noise Measurement**

The measurement of the input referred voltage noise of the parallel resonant tank with a  $Q$ -enhanced inductor posed a problem because of the  $50\text{-}\Omega$  measurement environment. Loading the high impedance  $Q$ -enhanced tank with  $50\text{-}\Omega$  degrades the  $Q$  and attenuates the input referred noise to a level where it is difficult to make a meaningful measurement. To address this problem, an external bipolar common emitter buffer amplifier with  $50\text{-}\Omega$  output impedance was placed between the tank and the spectrum analyzer used to measure the noise. A significant degradation in the tank  $Q$  was still observed using the bipolar buffer, but the loaded enhanced  $Q$  was still greater than the unloaded un-enhanced  $Q$  and the input noise was measurable.

Fig. 14 shows the measured input referred noise of the  $Q$ -enhancement circuit for five different enhanced  $Q$ 's along with the simulated input referred noise for the three-highest values of the loaded enhanced  $Q$ . The noise contribution of the buffer was also included in the simulation. The agreement between simulation and measurement was obtained by fitting the loaded  $Q$  in the simulation to the measurement.

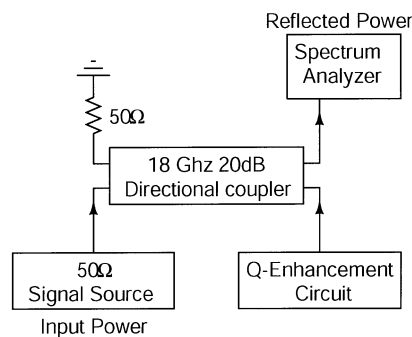


Fig. 15. Reflected distortion measurement setup.

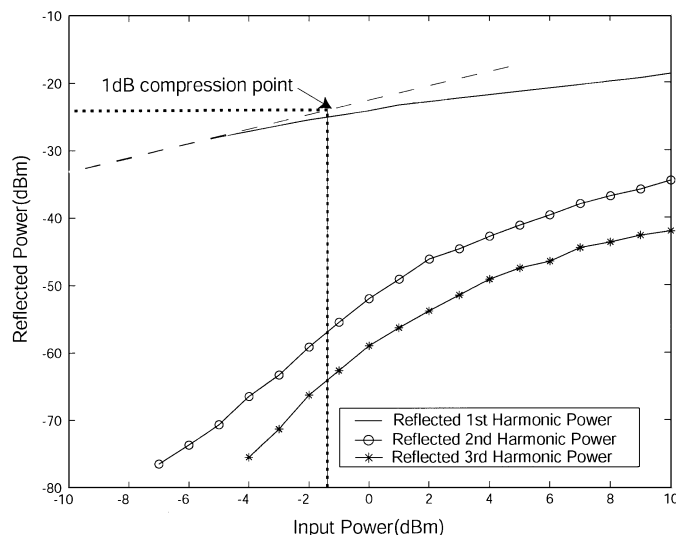


Fig. 16. Measured 1-tone harmonic distortion for  $Q = 200$ .

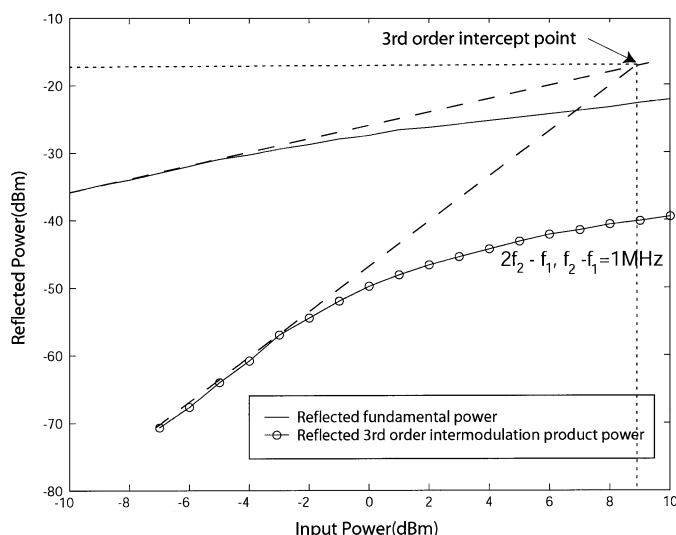


Fig. 17. Measured two-tone intermodulation distortion for  $Q = 200$ .

**C. Linearity Measurement**

A practical method of measuring the linearity performance of the circuit is to drive the tank with a  $50\text{-}\Omega$  power source and to measure the harmonic content of the power drawn by the circuit. Due to the impedance mismatch between the  $50\text{-}\Omega$  source and the high-impedance  $Q$ -enhanced tank, a directional coupler

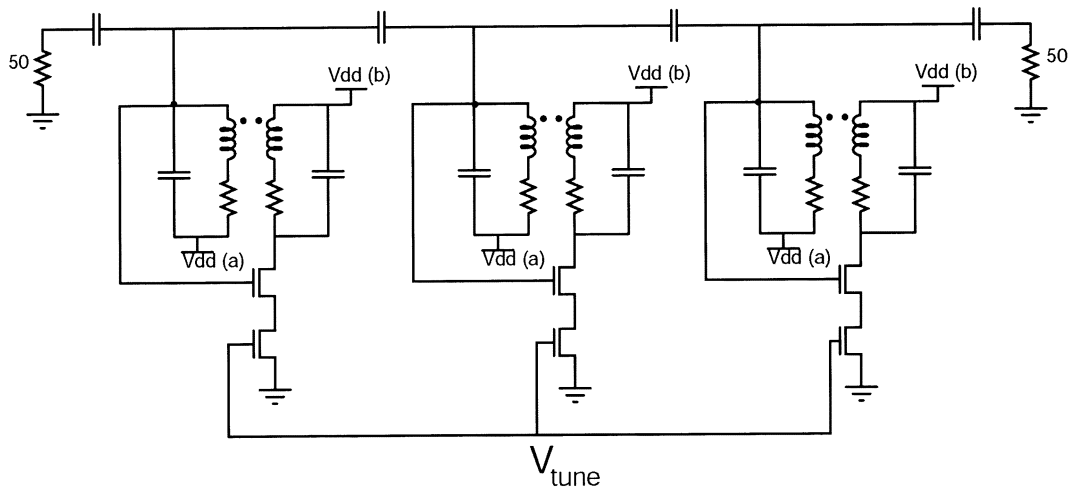


Fig. 18. Proposed application of the  $Q$ -enhancement technique to a coupled resonator bandpass filter.

is required to isolate the power incident on the tank from the reflected power as shown in Fig. 15.

A measurement analogous to the 1-dB compression point of the circuit can be obtained by sweeping the input power to the tank and measuring the reflected power. Since the impedance of the tank at resonance is essentially an open circuit compared to  $50\ \Omega$ , the reflection coefficient at the device is almost unity. The reflected power measured at the spectrum analyzer is, therefore, the incident power reduced by the attenuation through the directional coupler and the cables, which was 21.5 dB in our measurement setup. As the input power is increased, the input impedance presented by the  $Q$ -enhanced tank begins to drop due to nonlinear effects, which can be observed when the reflected power no longer depends on the input power in a linear fashion as shown in Fig. 16. Second- and third-order harmonic components are also observed. At the 1-dB compression point, the incident power to the device is  $-2.5$  dBm corresponding to an rms voltage swing of 167 mV. Since the device is essentially open circuit, the voltage will be double this value, i.e., 334 mV.

A measurement analogous to the third-order intercept point of the circuit can be obtained by sweeping a two-tone input power to the tank and measuring the third-order intermodulation products. This was measured using the setup shown in Fig. 15 where the signal source was replaced with two signal sources combined to produce a two-tone signal centered at the tank resonant frequency and spaced 1-MHz apart. The results are shown in Fig. 17. At the IP3 intercept point the measured reflected power at the spectrum analyzer was  $-16.5$  dBm, corresponding to signal power of  $+5$  dBm at the device. The voltage swing at the IP3 intercept is, therefore, approximately 800-mV rms.

#### IV. APPLICATION TO MONOLITHIC FILTERS

Soorapanth and Wong [4] have demonstrated the application of a  $Q$ -enhanced series-resonant circuit to the realization of a bandpass-filter structure, requiring an array of RF chokes to provide dc bias to the circuit. The use of the  $Q$ -enhanced parallel LC tank in the design of a monolithic series-C coupled resonator bandpass filter is shown in Fig. 18.

The capacitor values required to realize a bandpass filter centered at 2.44 GHz with a bandwidth of approximately 100 MHz are in the 200–5-pF range. The corresponding inductors have values of 2 nH. With the tuning FET eliminated and the inductors enhanced to a high- $Q$  value, the filter achieves a simulated insertion loss of approximately 0 dB in the passband, a noise figure of 23 dB, and an IP3 of  $-15$  dBm, consuming 3 mA from a 1.8-V supply. This performance is comparable to that presented in [4]. The proposed circuit may be biased without RF chokes. The simulations indicated that including the tuning FET has the benefit of facilitating the tradeoff between noise and linearity versus power consumption as it provides one more degree of freedom for the designer. The weaknesses of the circuit remain the small tolerances required for the capacitor values, distortion and the need for precision biasing. To overcome the precision biasing problem, self-tuning circuits can be used as shown in [4]. To overcome second-order distortion a differential implementation of the M1-M2 circuit may be employed.

#### V. CONCLUSION

A tunable  $Q$ -enhancement technique for monolithic spiral inductors in parallel resonant LC tanks has been presented. Electrical behavior, stability, noise, and distortion were described. The circuit was fabricated in a  $0.18\text{-}\mu\text{m}$  CMOS logic process with a low-resistivity epitaxial substrate. The measured input reflection coefficient and input referred noise of the  $Q$ -enhanced LC tank agreed well with simulated results. Tunability of the enhanced  $Q$  was also demonstrated and two stabilization techniques were proposed. The tunability of the  $Q$  factor of the parallel resonant tank facilitates its potential use in automatically tuned RF coupled resonator filter structures.

#### ACKNOWLEDGMENT

The authors thank M. Okoniewski and R. Randall for helpful discussions and assistance with some of the measurements. Thanks are also due to the reviewers for useful comments.

REFERENCES

- [1] C. P. Yue and S. S. Wong, "On-chip spiral inductors with patterned ground shields for Si-based RF IC's," *IEEE J. Solid-State Circuits*, vol. 33, pp. 743–752, May 1998.
- [2] A. Elshabini-Riad, W. B. Kuhn, and F. W. Stephenson, "Centre-tapped spiral inductors for monolithic bandpass filter," *Electron. Lett.*, vol. 1, no. 1, pp. 625–626, Jan. 1995.
- [3] Y. Cao, R. A. Groves, X. Huang, N. D. Zamdmer, J. O. Plouchart, R. A. Wachnik, T.-J. King, and C. Hu, "Frequency-independent equivalent-circuit model for on-chip spiral inductors," *IEEE J. Solid-State Circuits*, vol. 38, pp. 419–426, 2003.
- [4] T. Soorapanth and S. S. Wong, "A 0-dB IL 2140 ± 30 MHz bandpass filter utilizing  $Q$ -enhanced spiral inductors in standard CMOS," *IEEE J. Solid State Circuits*, vol. 37, pp. 579–586, May 2002.
- [5] K. W. Martin, R. Duncan, and A. Sedra, "A  $Q$ -enhanced active- $RLC$  bandpass filter," *IEEE Trans. Circuits Syst.*, vol. 44, pp. 341–346, May 1997.
- [6] D. Li and Y. Tsvividis, "Active LC filters on silicon," *Proc. Inst. Elect. Eng. Circuits Devices Syst.*, vol. 147, no. 1, pp. 49–56, Feb. 2000.
- [7] D. R. Pehlke, A. Burstein, and M. F. Chang, "Extremely high- $Q$  tunable inductor for Si-based RF integrated circuit applications," in *Proc. IEDM*, Washington, D.C., Dec. 1997, pp. 63–66.
- [8] Y.-C. Wu and M. F. Chang, "On-chip high- $Q$  (>3000) transformer-type spiral inductors," *Electron. Lett.*, pp. 112–113, Jan. 2002.
- [9] F. Albertoni, L. Fanucci, B. Neri, and E. Sentieri, "Tuned LNA for RFIC's using boot-strapped inductor," in *Proc. IEEE RFIC Symp.*, Phoenix, AZ, May 2001, pp. 83–86.
- [10] T. H. Lee, *The Design of CMOS Radio-Frequency Integrated Circuits*. Cambridge, U.K.: Cambridge Univ. Press, 1998.
- [11] A. J. Scholten, L. F. Tiemeijer, R. Langevelde, R. J. Havens, A. T. A. Z. van Duijnhoven, and V. C. Venezia, "Noise modeling for RF CMOS circuit simulations," *IEEE Trans. Electron. Devices*, vol. 50, pp. 618–632, 2003.
- [12] D. Pancini, G. Nicollini, and S. Pernici, "Simulation-oriented noise model for MOS devices," *IEEE J. Solid-State Circuits*, vol. SC-22, pp. 1209–1212, Feb. 1987.



**Bogdan Georgescu** (S'01) received the B.S.E.E. degree, with distinction, from the University of Calgary, Calgary, AB, Canada, in 2000. He is currently working toward the M.Sc. degree at the same university.

From 1997 to 2000, he was with Information Technologies, University of Calgary, working as a Programmer Analyst. In 2000, he joined the University of Calgary and TR Labs, Calgary. His research interests include the modeling and improvement of the quality of passive monolithic elements for RF integrated circuits.

egrated circuits.



**Holly Pekau** (S'03) received the B.S.E.E. (Hon.) degree from McGill University, Montreal, QC, Canada in 1997, and the M.S.E.E. degree from Northeastern University, Boston, MA, in 2001. She is currently working toward the Ph.D. degree at the University of Calgary, Calgary, AB, Canada.

From 1997 to 1999, she was with Analog Devices in Boston, MA, working on RF integrated circuits for CDMA applications. From 1999 to 2002, she was with IBM Microelectronics as a Staff Scientist in the Communications Research Design Center, Boston, MA, where she designed RF integrated circuits for GSM and WCDMA handsets. In 2003, she joined the University of Calgary and TR Labs, Calgary.



**James Haslett** (S'64–M'66–SM'79–F'02) received the B.Sc. degree in electrical engineering from the University of Saskatchewan, Saskatoon, SK, Canada, in 1966, and the M.Sc. and Ph.D. degrees from the University of Calgary, Calgary, AB Canada in 1968 and 1970, respectively.

In 1970, he joined the Department of Electrical Engineering, University of Calgary, where he is currently a Professor, and from 1986 to 1997, was Head of the Department. Since 1981, he has been president of his own consulting firm, consulting for oilfield instrumentation firms on high-temperature downhole instrumentation. In the 1970s and 1980s, he worked with several national and international science teams designing satellite instrumentation. In 1997, he joined TR Labs, Calgary, Industrial Research Consortium, Calgary. He currently holds the TR Labs/iCORE/NSERC Industrial Research Chair in Wireless RF IC Design. He has authored or co-authored more than 120 publications in the field of analog electronics, has written more than 40 technical reports for industry. His current research interests include high-temperature electronics for instrumentation applications, solid state imagers for scientific applications, biomedical microsystems and nanosystems, and RF microelectronics for telecommunications. He is an Associate Editor for the *Canadian Journal of Electrical and Computer Engineering*.

Dr. Haslett is a Fellow of the Engineering Institute of Canada. He has won 14 teaching awards in the past ten years. He is a Member of the Association of Professional Engineers, Geologists, and Geophysicists of Alberta, the Canadian Astronomical Society, the Canadian Society of Exploration Geophysicists, and the American Society for Engineering Education. He is currently a Member of the Editorial Review Committee of the IEEE TRANSACTIONS ON INSTRUMENTATION AND MEASUREMENT,



**John McRory** (M'86) received the B.Sc. degree in electrical engineering from the University of Alberta, Edmonton, AB, Canada in 1986, and the M.Eng. and Ph.D. degrees from the University of Calgary, Calgary, AB, in 1993 and 1997, respectively.

In 1986, he joined NovAtel Communications, Calgary, AB, where he worked in several design and management positions. In 1992 he joined TR Labs, Calgary, as a Staff Researcher, and is currently the Director of Operations for TR Labs, a Calgary based wireless research center. He is also an

Adjunct Professor in the Department of Electrical and Computer Engineering, University of Calgary. His current research interests include linear RF power amplifiers and nonlinear systems.